A. Tamer, P. Masarati
Stability of Nonlinear, Time-Dependent Rotorcraft Systems Using Lyapunov Characteristic Exponents
Journal of the American Helicopter Society, Vol. 61, N. 2, 2016, 022003 (12 pages)
doi:10.4050/JAHS.61.022003

Stability of Nonlinear, Time-Dependent Rotorcraft Systems Using Lyapunov Characteristic Exponents

Aykut Tamer

Ph.D. Fellow,

aykut.tamer@polimi.it,

Politecnico di Milano, Milano, Italy

Pierangelo Masarati

Associate Professor,

pierangelo.masarati@polimi.it,

Politecnico di Milano, Milano, Italy

Abstract

This work discusses the use of Lyapunov Characteristic Exponents to generalize rotorcraft stability analysis. Stability analysis of linear time invariant and time periodic systems relies on the eigenanalysis of special state transition matrices, which require the simplification of the nonlinear, time-dependent equations that govern rotorcraft aeromechanics. Lyapunov Characteristic Exponents provide quantitative information on the stability of nonlinear, time-dependent but not necessarily periodic dynamic systems without requiring a special reference solution. Results are consistent with the eigensolution of linear time invariant and Floquet-Lyapunov analysis of linear time periodic systems. Thus, the proposed approach represents a natural generalization of conventional stability analysis. The Discrete QR method is used to practically estimate Lyapunov Characteristic Exponents; its economy-size variant is considered to reduce the computational cost for large problems. The method is applied to rotorcraft-related problems; when possible, results are compared with usual methods for

Presented at the American Helicopter Society 71st Annual Forum, Virginia Beach, VA, May 5–7, 2015.

linear time invariant and time periodic problems.

Notation

$\mathbf{A}$	linear state space matrix	
$\mathbf{B}$	exponent matrix of Floquet-Lyapunov solution	
c	non-dimensional chord	
C'	lift deficiency function	
C_d	nominal blade damping constant	$\mathrm{N\,m\,s\,rad^{-1}}$
C_L	damping at zero lag rate of nonlinear damper	$\mathrm{N\,m\,s\,rad^{-1}}$
e_f	flap hinge offset	m
$\mathbf{f}$	differential problem	
f_c	control moment	$\mathrm{N\,m}$
f_d	damping moment	$\mathrm{N\,m}$
$\mathbf{H}$	monodromy Matrix	
$\mathbf{I}$	identity matrix	
I_b	$\int_0^R r^2 m \mathrm{d}r$ blade inertia per unit length	$\mathrm{kg\,m}$
I_θ	distribution of blade feathering inertia per unit length	$\mathrm{kg\,m}$
$\hat{I}_f$	$\int_0^R I_\theta \mathrm{d}r / I_b$ non-dimensional feathering inertia	
$\hat{I}_x$	$\int_0^R x_I r m \mathrm{d}r / I_b$, non-dimensional inertial coupling	
$\hat{I}_\beta$	$\int_{e_f}^R x_I r m \mathrm{d}r / I_b$ non-dimensional flap inertia	
K_p	$\tan\delta_3$, structural pitch-flap coupling	
m	mass distribution per unit length	$\mathrm{kg\,m^{-1}}$
$m_\spadesuit$	non-dimensional pitching moment with respect to ($\spadesuit$)	
$M_\spadesuit$	non-dimensional flap moment with respect to ($\spadesuit$)	
$\mathbf{P}(t)$	periodic matrix of Floquet-Lyapunov solution	
$\mathbf{Q}$	orthogonal matrix satisfying $\mathbf{QR} = \mathbf{M}$ of a generic matrix $\mathbf{M}$	
$\mathbf{R}$	upper triangular matrix satisfying $\mathbf{QR} = \mathbf{M}$ of a generic matrix $\mathbf{M}$	

$\mathbf{R}_{\Pi_i}$	accumulated matrix $\mathbf{R}$ of discrete QR algorithm	
r	radial coordinate r	m
r_{ii}	ith diagonal element of matrix $\mathbf{R}$	
t	time	s
T	fundamental period of a periodic system	s
$\mathbf{x}$	vector of state variables	
$\mathbf{Y}$	state transition matrix	
${}_i\mathbf{x}$	ith state variables vector of problem linearized about fiducial trajectory	
x_A	non-dimensional aerodynamic center offset	
x_I	chordwise center of mass offset	m
β	flap angle	rad
γ	Lock number	
δ_{FP}	half freeplay region	rad
δ_3	structural pitch-flap coupling angle	rad
ζ	lead-lag angle	rad
θ	control surface deflection	rad
θ_l, θ_u	lower and upper boundaries of freeplay	rad
λ_i	ith Lyapunov Characteristic Exponent (LCE)	s^{-1}
μ	advance ratio	
ν_β	non-dimensional flap frequency	
ξ_A	x_A/c, non-dimensional aerodynamic offset normalized by chord	
χ	coefficient of the quadratic term of nonlinear damper	$\mathrm{Nms}^2/\mathrm{rad}^2$
$\bar{\chi}$	saturation of nonlinear damper	$\mathrm{Nms}^2/\mathrm{rad}^2$
ω_θ	non-dimensional pitch frequency	
$(\clubsuit)_{/(\spadesuit)}$	partial derivative of $(\clubsuit)$ with respect to $(\spadesuit)$	

Introduction

This work presents the use of Lyapunov Characteristic Exponents (LCE), or Lyapunov Exponents in short, to evaluate the stability of solutions of aeromechanics problems entailing rotorcraft modeled as a system of nonlinear, time-dependent (often termed *non-autonomous*) differential equations of the form

$$\dot{\mathbf{x}} = \mathbf{f}(\mathbf{x}, t), \tag{1}$$

with $\mathbf{x} \in \mathbb{R}^n$, $\mathbf{f} : \mathbb{R}^{n+1} \to \mathbb{R}^n$ and $t \in \mathbb{R}$.

Stability is a key problem in rotorcraft aeromechanics. The modern stability theory is deeply rooted into Aleksandr M. Lyapunov's seminal work (Ref. 1). The theory of linear, time-invariant (LTI) and time-periodic (LTP) problems

$$\dot{\mathbf{Y}}(t, t_0) = \mathbf{A}(t)\mathbf{Y}(t, t_0), \qquad \mathbf{Y}(t_0, t_0) = \mathbf{I} \tag{2}$$

with $\mathbf{A}(t) = \mathbf{f}_{/\mathbf{x}}$ respectively constant or periodic (i.e. $\mathbf{A}(t + T) \equiv \mathbf{A}(t)\ \forall t \in \mathbb{R}$), is complete. Their solution is a state transition matrix (STM) $\mathbf{Y}(t, t_0)$ from time t_0 to t, which is exponential (a space of constant or periodic vectors representing the principal directions in the state space, each multiplied by the corresponding characteristic exponential),

$$\mathbf{x}(t) = \mathbf{P}(t)\mathrm{e}^{\mathbf{B}(t-t_0)}\mathbf{x}_0 \tag{3}$$

with $\mathbf{x}_0 = \mathbf{x}(t_0)$, $\mathbf{P}(t + T) = \mathbf{P}(t)$ and $\mathbf{P}(0) = \mathbf{I}$, and $\mathbf{B}$ constant. The evolution of a perturbed solution is determined by the real part of the exponents that characterize the solution, i.e. the eigenvalues of the constant matrix $\mathbf{B}$, which is equivalent to matrix $\mathbf{A}$ for LTI problems, and, according to the Floquet-Lyapunov theory for LTP problems, is the matrix that characterizes the monodromy matrix $\mathbf{H} = \mathrm{e}^{\mathbf{B}T}$, which corresponds to the STM over one period T, namely $\mathbf{H} = \mathbf{Y}(t + T, t)$.

The stability of equilibrium points of nonlinear, time-invariant problems can be evaluated by considering a linearization about the points themselves, according to the Hartman-Grobman theorem (Ref. 2), when the real part of the eigenvalues of $\mathbf{f}_{/x}$ is non zero; the Center Manifold theorem (Ref. 3) can be used otherwise. Similarly, when the problem is nonlinear and time-dependent but specifically time-periodic, the stability of periodic orbits can be evaluated using the Floquet-Lyapunov theory after linearization about those orbits.

This is well known in the rotary wing community since LTI and LTP approximations are often considered acceptable, especially when stability is addressed. The seminal work of Parkus (Ref. 4), who first used Floquet-Lyapunov analysis in blade flapping aeromechanics, thanks to the advent of digital computers was later applied by Peters and Hohenemser (Ref. 5) to practical models, followed by others, see for example References 6–8. However, LTI and LTP approximations may not be always acceptable; furthermore, the related methods require the knowledge of special solutions (equilibrium points or orbits) and, in the case of LTP problems, of the period of the system, which may not be always readily available.

The dynamics of rotorcraft is generally described by nonlinear, time-dependent equations (Ref. 9); its representation as LTI and LTP systems imply simplifications for nonlinear and aperiodic systems. In fact, rotorcraft can be considered periodic systems only when their rotors operate at constant angular velocity. Moreover, in case of rotors operating at different angular velocities, as for the conventional main/tail rotor arrangement, the actual period is the least common multiple of all rotors' periods. In special cases, e.g. when limit cycle oscillations (LCO) arise, the periodicity resulting from the time dependence of the problem is destroyed by the presence of natural oscillations with a period that is usually incommensurable with that of the problem itself. The interest for this kind of problems is growing also in the rotorcraft industry (Ref. 10).

A method is sought that: 1) provides information about the stability of arbitrary solutions of nonlinear, time-dependent systems, 2) is consistent with usual criteria for LTI and LTP problems, and 3) is computationally robust. LCEs satisfy these criteria (Ref. 11). Specifically, LCEs can estimate the stability properties of generic solutions of the problem directly during their computation. Despite possessing many of the desired characteristics, to the authors' knowledge they have not yet been used to evaluate the stability of rotorcraft problems.

This work briefly presents the theory of LCEs and practical algorithms for their estimation, discussing improvements needed to meet the requirements and outlining strategies for their achievement. Stability analysis using LCEs is illustrated for typical rotorcraft aeromechanics problems; the resulting stability indicators are compared with the corresponding ones obtained by conventional methods, when possible.

Lyapunov Characteristic Exponents

LCEs represent the rate of expansion or contraction of perturbations of a generic solution along independent directions in the state space. As such, they represent stability indicators associated with each of these directions.

Consider a solution $\mathbf{x}(t)$ of Eq. (1) for $t \geq t_0$, often called 'fiducial trajectory', and a solution ${}_i\mathbf{x}(t)$ of the problem

$$ {}_i\dot{\mathbf{x}} = \mathbf{f}_{/\mathbf{x}}\big|_{\mathbf{x}(t),t}\, {}_i\mathbf{x}, \qquad {}_i\mathbf{x}(t_0) = {}_i\mathbf{x}_0 \tag{4} $$

for arbitrary ${}_i\mathbf{x}_0$. LCEs are defined as

$$ \lambda_i = \lim_{t\to\infty} \frac{1}{t} \log \left\| {}_i\mathbf{x}(t) \right\| , \tag{5} $$

where each λ_i is calculated from one of n linearly independent ${}_i\mathbf{x}_0$ that represent the equivalent of the principal directions of an LTI problem. Since Eq. (4) is linear time-dependent, its solution can be written as

$$ {}_i\mathbf{x} = \mathbf{Y}(t, t_0)\, {}_i\mathbf{x}_0 \tag{6} $$

where $\mathbf{Y}(t, t_0)$ is the solution of $\dot{\mathbf{Y}} = \mathbf{f}_{/\mathbf{x}}\big|_{\mathbf{x}(t),t} \mathbf{Y}$, with $\mathbf{Y}(t_0, t_0) = \mathbf{I}$, namely the problem's STM from t_0 to t. Then Eq. (5) is equivalent to

$$ \lambda_i = \lim_{t\to\infty} \frac{1}{t} \mathrm{Re} \left(\log \left(\mathrm{eig} \left(\mathbf{Y}(t, t_0) \right) \right) \right) . \tag{7} $$

When all LCEs are negative, the solution is exponentially stable. When at least one LCE is positive, the solution is unstable, or leads to a chaotic attractor. When the largest LCE is zero, or the largest LCEs are zero, a LCO is expected; i.e., there exists a direction in the state space along which the solution neither expands nor contracts. In case of multiple largest LCEs equal to zero, a higher order periodic or quasi-periodic attractor exists, e.g. a torus.

Note the analogy with the LTI case, since $\mathbf{Y}(t, t_0) \overset{\text{LTI}}{\equiv} \mathrm{e}^{\mathbf{A}(t-t_0)}$ and thus $\lambda_i \overset{\text{LTI}}{=} \mathrm{Re}(\mathrm{eig}(\mathbf{A}))$, and with the LTP one, in which

$$ \lambda_i \overset{\text{LTP}}{=} \frac{1}{T} \mathrm{Re} \left(\log \left(\mathrm{eig} \left(\mathbf{Y}(t_0 + T, t_0) \right) \right) \right) . \tag{8} $$

LCEs are often called the 'spectrum' of a problem, inasmuch as the eigenvalues of matrix $\mathbf{A} = \mathbf{f}_{/\mathbf{x}}$ define the spectrum of a LTI problem.

Eq. (7) is not practical, because usually the elements of the STM either contract to zero or expand to infinity, depending on the (lack of) stability of the solution, thus either over- or underflowing. The practical computation of LCEs requires one to exploit re-orthogonalization of local directions of evolution of the solution, as proposed in the seminal work of Benettin *et al.* (Ref. 12), which first showed that the computation of LCEs could be practically and effectively achieved. Alternative formulas have been proposed, based on well known orthogonal decompositions (SVD and QR, respectively):

$$\lambda_i = \lim_{t\to\infty} \frac{1}{t} \log\left(\mathrm{svd}\left(\mathbf{Y}(t,t_0)\right)\right) = \lim_{t\to\infty} \frac{1}{t} \log\left(\mathrm{diag}\left(\mathrm{qr}\left(\mathbf{Y}(t,t_0)\right)\right)\right), \tag{9}$$

Efficient algorithms are available; for example, the continuous SVD and QR methods, and the discrete QR method (Refs. 12–14). However, those decompositions have trouble with LCEs of multiplicity greater than one. This case, frequent in mechanics, intuitively corresponds to subcritically damped oscillatory systems, whose complex conjugated eigenvalues share the same real part. As discussed in Ref. 15, the computability of an LCE requires that the problem possesses the property of exponential dichotomy, which in turn requires an appropriate separation from the other LCEs.

The possibility to extend the approach to systems of differential-algebraic equations, as outlined for example in Refs. 16–21, represents a promising development, in view of their use in the formulation of modern multibody dynamics.

The Discrete QR Method

The definitions of Eqs. (7) and (9) can hardly be applied to the practical estimation of LCEs, because some sort of orthogonalization is needed to prevent the solution for each axis of the ellipsoid from interfering with the others. Numerical methods have been devised for this purpose. One of the most popular is the so-called Discrete QR method. It is based on incrementally updating the LCE estimates with the diagonal elements of the upper-triangular matrix $\mathbf{R}$ obtained from the QR decomposition of the STM between two consecutive time steps.

Given the previously mentioned STM $\mathbf{Y}(t,t_{j-1})$ from time t_{j-1} to an arbitrary time t, set $\mathbf{Y}_j =$

$\mathbf{Y}(t_j, t_{j-1})$. Consider then the QR decomposition (Ref. 22) of $\mathbf{Y}_j\mathbf{Q}_{j-1}$, starting from $\mathbf{Q}_0 = \mathbf{I}$, which implies $\mathbf{Q}_j\mathbf{R}_j = \mathbf{Y}_j\mathbf{Q}_{j-1}$. Now, after defining $\mathbf{R}_{\Pi_j} = \Pi_{k=0}^{j}\mathbf{R}_{j-k}$, one can show that

$$\mathbf{Y}_j\mathbf{Q}_{j-1}\mathbf{R}_{\Pi_{j-1}} = \mathbf{Q}_j\mathbf{R}_j\mathbf{R}_{\Pi_{j-1}} = \mathbf{Q}_j\mathbf{R}_{\Pi_j}. \tag{10}$$

This way, $\mathbf{Y}_j\mathbf{Q}_{j-1}\mathbf{R}_{\Pi_{j-1}}$ can be used to construct the QR decomposition of the STM from t_0 to t_j as $\mathbf{Y}(t_j, t_0) = \mathbf{Q}_j\mathbf{R}_{\Pi_j}$ by only considering incremental QR decompositions over $\mathbf{Y}_k\mathbf{Q}_{k-1}$, i.e. with limited contraction/expansion in matrices $\mathbf{R}_k$. The LCEs are then estimated from $\mathbf{R}_{\Pi_j}$ as

$$\lambda_i = \lim_{j\to\infty} \frac{1}{t_j} \log r_{ii}(t_j), \tag{11}$$

where $j \in \mathbb{N}$ and $r_{ii}(t_j)$ are the diagonal elements of matrix $\mathbf{R}(t_j) = \mathbf{R}_{\Pi_j}$, since the product of two upper triangular matrices $\mathbf{C} = \mathbf{AB}$ is also an upper triangular matrix, whose diagonal elements are $c_{ii} = a_{ii}b_{ii}$. Thus the logarithm of c_{ii} can be incrementally computed as $\log(a_{ii}b_{ii}) = \log(a_{ii}) + \log(b_{ii})$. This helps preventing overflow/underflow in numerical computations. Furthermore,

$$r_{ii}(t_j) = \Pi_{k=0}^{j} r_{(j-k)_{ii}}, \tag{12}$$

thus

$$\log\left(r_{ii}(t_j)\right) = \sum_{k=0}^{j} \log(r_{k_{ii}}), \tag{13}$$

which leads to

$$\lambda_i = \lim_{j\to\infty} \frac{1}{t_j} \sum_{k=0}^{j} \log(r_{k_{ii}}). \tag{14}$$

Care must be taken to ensure that the diagonal elements of $\mathbf{R}_j$ are positive, which can be satisfied by changing the sign of the corresponding column of the $\mathbf{Q}$ matrix.

The need to perform lengthy simulations to attain convergence of LCE estimates is perhaps the main limitation to the practical usage of the proposed approach. In terms of comparison, LTI problems only require the computation of the eigenvalues of a matrix, whose cost is of the order of n^4 for a dense matrix of size n. LTP problems additionally require the computation of the monodromy matrix, whose cost, when performed using explicit schemes, is $O(n^2p)$, being p the number of time steps in which the period is divided. The cost of the discrete QR algorithm is that of time integration over several periods, and of repeated QR decompositions. The latter is $O(n^3)$. When n is large, this problem can be mitigated using

the so-called economy-size QR decomposition, also called the *thin* (Ref. 22), or *reduced* (Ref. 23) QR decomposition. As discussed for example in Ref. 24, consider the QR decomposition of a rectangular matrix $\mathbf{M} \in \mathbb{R}^{n\times q}$, with $q < n$ such that n represents the size of the problem and q is the number of required LCE estimates. Then

$$\mathbf{QR} = \mathbf{M} = \begin{bmatrix} \mathbf{Q}' \, \mathbf{Q}'' \end{bmatrix} \begin{bmatrix} \mathbf{R}' \\ \mathbf{0} \end{bmatrix} = \mathbf{Q}'\mathbf{R}' \tag{15}$$

where the prime $(')$ indicates matrices associated with an arbitrary q-sized subspace of the state space of the problem. The economy-size QR decomposition is represented by $\mathbf{M} = \mathbf{Q}'\mathbf{R}'$, where $\mathbf{Q}' \in \mathbb{R}^{n\times q}$ and $\mathbf{R}' \in \mathbb{R}^{q\times q}$.

Consider now the economy-size QR decomposition of a partial STM $\mathbf{Y}'_j \in \mathbb{R}^{n\times q}$ obtained by integrating the evolution of a set of orthogonal vectors $\mathbf{Q}'$ that span an arbitrary subspace of the state space of the problem, i.e. formally the solution of integrating the problem $\dot{\mathbf{Y}}' = \mathbf{A}\mathbf{Y}'$ from t_{j-1} to t_j with initial conditions $\mathbf{Y}'(t_{j-1}) = \mathbf{Q}'_{j-1}$. In principle, $\mathbf{Y}'_j = \mathbf{Y}(t_j, t_{j-1})\mathbf{Q}'_{j-1}$. The diagonal elements of matrix $\mathbf{R}'_j$, accumulated according to the formula $\mathbf{R}'_{\Pi_j} = \Pi_{i=j}^{1}\mathbf{R}'_i$, thus evolve towards an estimate of the largest diagonal elements of matrix $\mathbf{R}_{\Pi_j}$ that refers to the complete state. An example that investigates the convergence and time saving issues of economy size QR decomposition is provided in next section.

Another problem that is common to all algorithms proposed so far for practical LCE estimation is related to the multiplicity of LCEs. Estimates of LCEs with multiplicity greater than one show a slow convergence rate and can, in some cases, fail to converge (Ref. 15). In problems of interest of mechanical and aerospace engineering it is common to have STMs with complex conjugated eigenvalues, which intuitively correspond to subcritically damped oscillators. Those cases lead to multiple LCEs, since they are related to the logarithm of the modulus of such complex conjugated eigenvalues.

It has been observed that in those cases considering the average of LCE estimates that appear to converge to the same value gives a much better estimation for lower values of the time at which estimation is truncated. Some of the numerical examples reported in the following make use of this technique to improve the estimation of LCEs which appear as pairs. More robust approaches for the detection of LCEs with multiplicity greater than one are being formulated by the authors.

Applications

In this Section, LCEs are applied to the study of the stability of rotorcraft-specific problems. The discrete QR method is used. The problems are first integrated in time using the implicit, second-order accurate, A/L stable (i.e. unconditionally stable, with algorithmic dissipation) multistep integration scheme recently discussed in [25]. Subsequently, the incremental STM across each time step is computed using a 'leapfrog' variant of the implicit second-order accurate, A-stable (i.e. unconditionally stable) Crank-Nicolson scheme: considering $\mathbf{x}_{k+1/2} = \mathbf{x}_{k-1/2} + h\dot{\mathbf{x}}_k$, where h is the time step, $\dot{\mathbf{x}}_k = \mathbf{A}(t_k)\mathbf{x}_k$, and $\mathbf{x}_k = (\mathbf{x}_{k+1/2} + \mathbf{x}_{k-1/2})/2$. In short,

$$\mathbf{x}_{k+1/2} = \left(\mathbf{I} - \frac{h}{2}\mathbf{A}(t_k)\right)^{-1}\left(\mathbf{I} + \frac{h}{2}\mathbf{A}(t_k)\right)\mathbf{x}_{k-1/2}, \tag{16}$$

where the matrix at the right-hand side is a second-order accurate approximation of the STM from $t_{k-1/2}$ to $t_{k+1/2}$ of a linear, time invariant problem, as discussed in [21]. Although this scheme is implicit, no iteration is needed because the problem is linear. Of course, other, more accurate schemes can be used as well.

Flapping Dynamics of a Helicopter Blade

The LCEs estimated for this linear time periodic example are compared with the characteristic exponents of the Floquet-Lyapunov Method. Under simplifying assumptions, the flapping of a single rigid rotor blade can be formulated as a second order single degree of freedom LTP problem (from Ref. 26). Since the purpose of this example is to compare LCEs and Floquet exponents for LTP systems, only periodicity is retained instead of using a more realistic but complex helicopter blade dynamics model. The model is simplified by linearizing the dynamics, using quasi-static aerodynamics and neglecting reverse flow conditions. The dots represent differentiation with respect to the azimuth angle t (in this context, it represents non-dimensional time). The equation of motion is

$$\ddot{\beta} + \frac{\gamma}{8}\left(1 + \frac{4}{3}\mu\sin(t)\right)\dot{\beta} + \left(\nu_\beta^2 + \frac{\gamma}{8}\left(\frac{4}{3}\mu\cos(t) + \mu^2\sin(2t)\right)\right)\beta = 0 \tag{17}$$

It represents the flapping of a rigid helicopter blade, where β is the blade flap angle, γ is the Lock number (the non-dimensional ratio between aerodynamic and inertial flapping loads, which in the present context

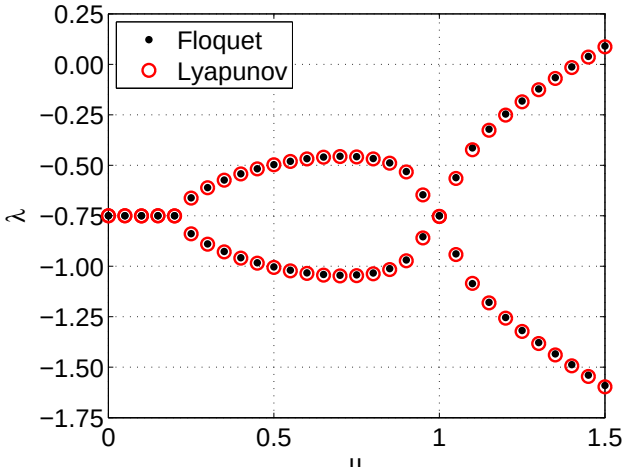

Fig. 1: Blade flapping: estimates of LCEs with respect to advance ratio μ.

is roughly proportional to 16 times the damping factor), μ is the advance ratio (the ratio between the helicopter forward velocity and the blade tip velocity in hover, which weighs the periodic part of the coefficients) and ν_β is the flapping frequency non-dimensionalized using the rotor angular velocity Ω.

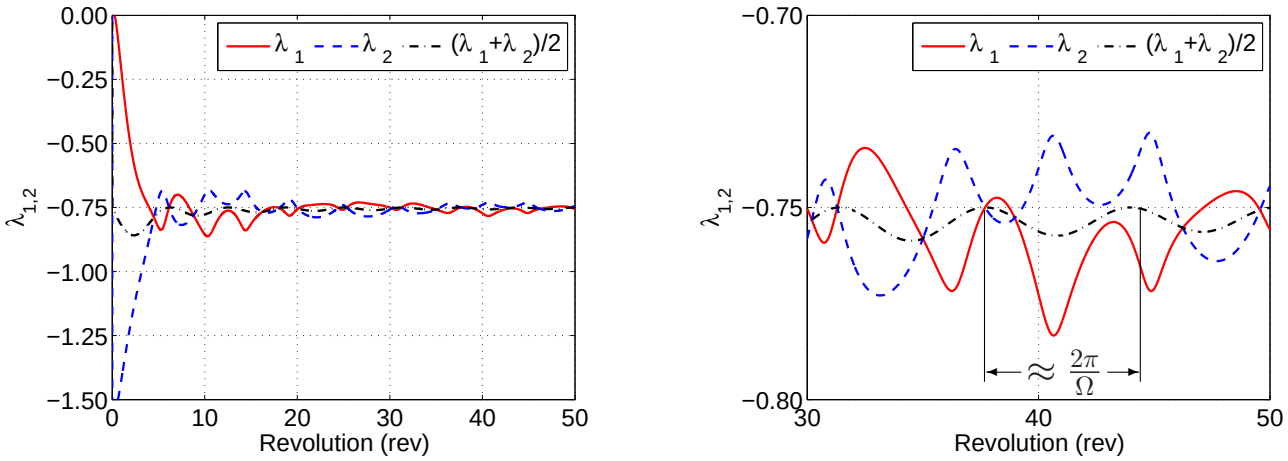

(a) Time evolution

(b) Zoomed after convergence

Fig. 2: Blade flapping: time evolution of LCE estimates and zoomed plot after convergence, $\mu = 0.15$

In order to illustrate the trend of LCE estimates with respect to a parameter, the advance ratio μ is chosen. The values of the Lock number and flapping natural frequency are set to $\gamma = 12$ and $\nu_\beta = 1$ respectively, whereas the rotor angular speed is considered as a normalized value, $\Omega = 1$. The LCE

estimates are compared in Fig. 1 with the corresponding values obtained using the Floquet-Lyapunov theory for a range of advance ratio $0 \leq \mu \leq 1.5$. Note that advance ratios in excess of 0.5 are way beyond the maximum values of conventional helicopters, but may be of interest for slowed rotors. Both results of Floquet-Lyapunov and LCE methods are in good agreement. Up to $\mu = 0.22$ the system has two complex conjugated characteristic exponents, whose equal real parts do not depend on μ. Beyond that value of μ, the periodic nature of the system leads to distinct real parts for the two LCEs, which vary with μ. Now the stability of one of the characteristic solutions increases, whereas that of the other one reduces.

The time evolution of LCE estimates associated with complex conjugated eigenvalues for $\mu = 0.15$ are shown in Fig. 2a; a detailed view is shown in Fig. 2b. Although each LCE estimate in Fig. 2a shows a rather erratic behavior, slowly converging to the corresponding Floquet exponent, their average appears to be much more regular. Owing to periodicity, it oscillates with the period of the system, $T = 2\pi$, about the expected value. The slow, hyperbolic decay is caused by the division by t that occurs in Eq. (5).

Computing the average of two LCE estimates corresponds to computing the evolution of

$$\frac{\lambda_1 + \lambda_2}{2} = \lim_{t \to +\infty} \frac{\log(r_{11}) + \log(r_{22})}{2t} = \lim_{t \to +\infty} \frac{\log(r_{11} r_{22})}{2t} \tag{18}$$

which can be interpreted as the rate of evolution of a subvolume of the state space consisting of the product of two directions, divided by the number of directions. When both directions evolve at the same rate, i.e. the LCE has multiplicity equal to 2, the average is exactly the value of the LCE.

In order to have an accurate estimate of the LCEs, integration needs to be performed for a long enough non-dimensional time to let the oscillations vanish; hence, such pairing of LCE estimates can help improving the convergence and robustness of the estimation. Computing the average of two LCE estimates is always legitimate; however, its interpretation is only meaningful when both LCE estimates converge to the same value. A development in this sense is being considered for a future work.

Helicopter Ground Resonance with Nonlinear Lead-Lag Dampers

Helicopter Ground Resonance (GR) is a mechanical instability associated with the in-plane degrees of freedom that describe the lead-lag motion of the rotor blades (see the seminal work by Coleman and Feingold, Ref. 27). The combination of the in-plane motion of the blades causes an overall in-plane

motion of the rotor center of mass which couples with the fixed frame pitch and roll dynamics of the airframe and undercarriage system. For this reason, the damping of the in-plane motion of the blades can be critical in articulated and soft-inplane rotor designs. Such damping is usually provided by lead-lag dampers.

The suitability and soundness of the proposed approach for the stability evaluation of non-trivial linear, time periodic problems was already illustrated in Ref. 28 by comparing LCEs with Floquet exponents for the dissimilar damper case proposed in Ref. 6. A distinctive advantage of LCEs is their capability to analyze and quantify the stability of generic trajectories of nonlinear, time-dependent dynamical systems. Among phenomena that are characteristic of nonlinear systems, LCOs are defined as isolated closed trajectories of nonlinear dynamical systems; when an LCO develops, the system oscillates in a self-sustained manner without the need of an external input, as described in Ref. 29. Being LCO bounded, at a first glance they seem to be less malign than the classical instability of linear systems, with respect to system integrity, in the sense that oscillations do not grow unbounded in amplitude. Nonetheless, the occurrence of LCOs can affect structural life, flight safety, and ride comfort of rotorcraft. As in the case of nonlinear phenomena, the occurrence of LCOs can only be detected considering the nonlinearity of the problem (Ref. 30). The proposed GR problem highlights the capability to determine the stability of the problem, including that of Limit Cycle Oscillations (LCO), without prior knowledge of any special (e.g. steady, or periodic) solution.

Owing to its simplicity, Hammond's model (Ref. 6) has been extensively used to study GR. The schematic is presented in Fig. 3 and the corresponding numerical values are given in Table 1. In this work, it is taken as the reference model with modified non-linear blade lead-lag damper characteristics.

The GR problem with nonlinear lead-lag dampers is of course nonlinear, although time-invariant due to the symmetry of the rotor when isotropic, i.e. having equally spaced blades with identical properties. Hammond's model is modified by using the nonlinear damper constitutive law illustrated in Ref. 31 and modified by adding a linear term to the quadratic one, namely

$$f_d = \begin{cases} \chi\dot{\zeta}|\dot{\zeta}| + C_L\dot{\zeta} & |\dot{\zeta}| < |\dot{\zeta}_L| \\ \bar{\chi}\dot{\zeta}_L|\dot{\zeta}_L| & |\dot{\zeta}| \geq |\dot{\zeta}_L| \end{cases} \tag{19}$$

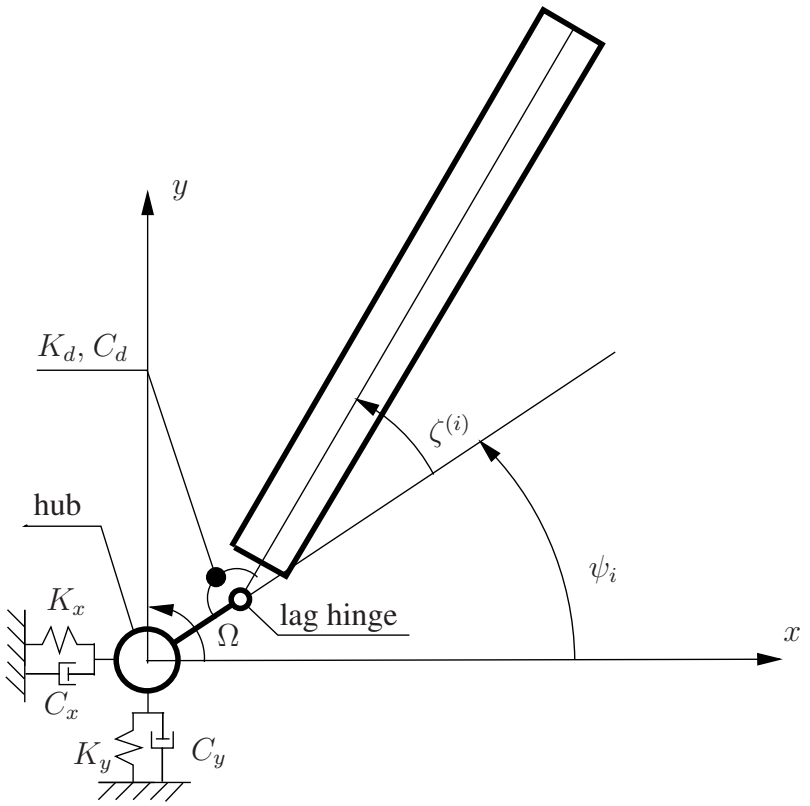

Fig. 3: Schematic of Hammond's helicopter ground resonance model; one blade is presented for clarity.

Table 1: Ground resonance: numerical values of Hammond model parameters (Ref. 6)

Number of blades	N	4	—
Blade static moment	S_ζ	189.1	kg·m
Blade moment of inertia	J_ζ	1084.7	kg·m^2
Lag hinge offset	e	0.3048	m
Lag spring	K_d	0.0	N·m·rad^{-1}
Lag damper	C_d	4067.5	N·m·s·rad^{-1}
Hub generalized mass	M_x	8026.6	kg
	M_y	3283.6	kg
Hub damper	C_x	51078.7	N·s·m^{-1}
	C_y	25539.3	N·s·m^{-1}
Hub spring	K_x	1240481.8	N·m^{-1}
	K_y	1240481.8	N·m^{-1}

where $\chi = \bar{\chi} - C_L/\dot{\zeta}_L$; numerical values are given in Table 2. The slope at zero lag rate, C_L, is varied from zero to the nominal value C_d of Hammond's model (Ref. 6). This problem has been selected to obtain a system with LCO in an otherwise reasonably realistic model (with more than one degree of freedom) and to test stability indications of LCE estimation with a nonlinear rotorcraft-related problem that may include LCO, exponential stability, and unstable equilibria.

Table 2: Helicopter ground resonance with nonlinear blade damper: saturated hydraulic damper parameters, data from Ref. 31.

$\bar{\chi}$	1.2203×10^6	N·m·s^2·rad^{-2}
$\dot{\zeta}_L$	1.0	deg·s^{-1}

Figure 4 shows the lag motion of one blade for the cases that experience LCO ($C_L = 0$, Fig. 4a) and exponential stability ($C_L = C_d$, Fig. 4b). Both plots show simulations starting from different initial conditions. The curves in Fig. 4a oscillate with the same period and amplitude; hence they converge to

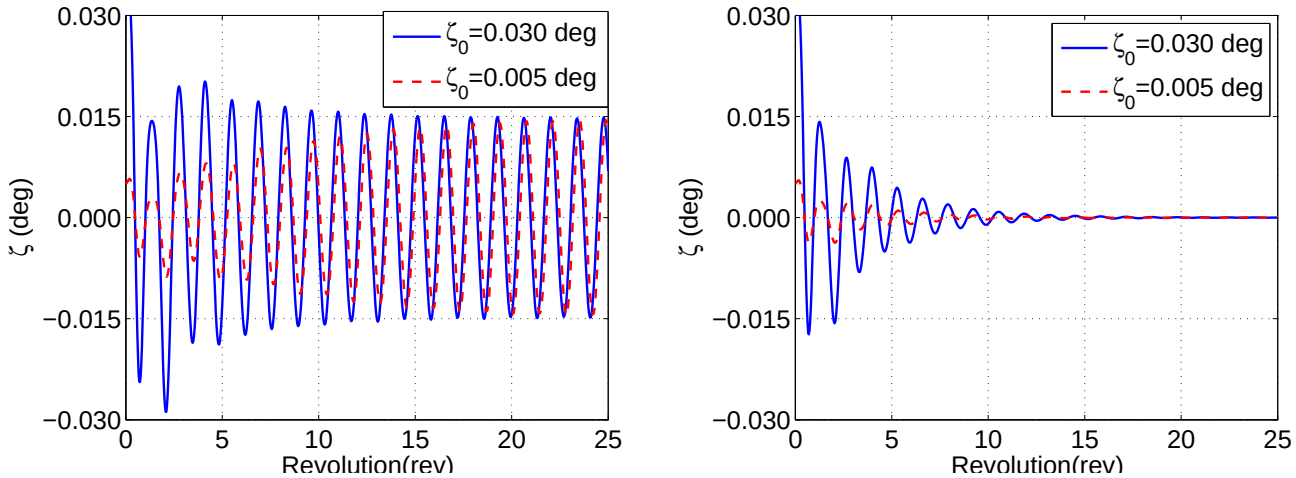

(a) LCO ($C_L = 0$)

(b) Exponentially stable ($C_L = C_d$)

Fig. 4: Helicopter ground resonance with nonlinear blade damper: blade lag motion starting from different initial conditions.

the same LCO, although a phase difference can be observed as a consequence of the initial conditions. It is worth noticing that the trivial solution $\zeta = 0$ is also an equilibrium solution; however, since solutions obtained with initial conditions close to $\zeta = 0$ converge to the LCO rather than vanishing, $\zeta = 0$ is topologically an unstable equilibrium point. The present analysis for such fiducial trajectory estimates a positive largest LCE, confirming its instability when $C_L = 0$. On the contrary, Fig. 4b shows that when

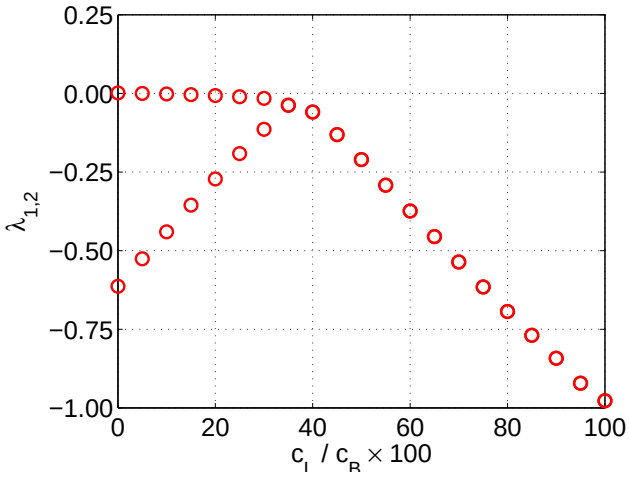

Fig. 5: Helicopter ground resonance with nonlinear blade damper: largest two LCE estimates vs. damper slope at zero lag rate C_L.

$C_L = C_d$, the resulting curves converge to $\zeta = 0$, confirming that such fiducial trajectory is now a stable point.

LCE estimates equal to zero are expected for systems with an LCO. LCEs are estimated for a range of damper slope at zero lag rate, C_L ($C_L = 0$ was used in Ref. 31) and presented in Fig. 5. It can be observed that the largest LCE is zero up to $C_L/C_d \approx 35\%$, indicating LCO for this range of the parameter. For larger values of C_L, the two largest LCEs (nearly) merge (i.e. they become quite close from a numerical point of view) and the fiducial trajectory becomes exponentially stable with all LCEs negative. This is verified in Fig. 4a: the largest LCE estimate equal to zero indicates convergence to a stable LCO with magnitude 0.015 deg, with the corresponding time evolution of the largest two LCEs given in Fig. 6a. In Fig. 4b, with all LCEs negative, the motion is exponentially stable. The time evolution of the largest two LCEs for this case is presented in Fig. 6b.

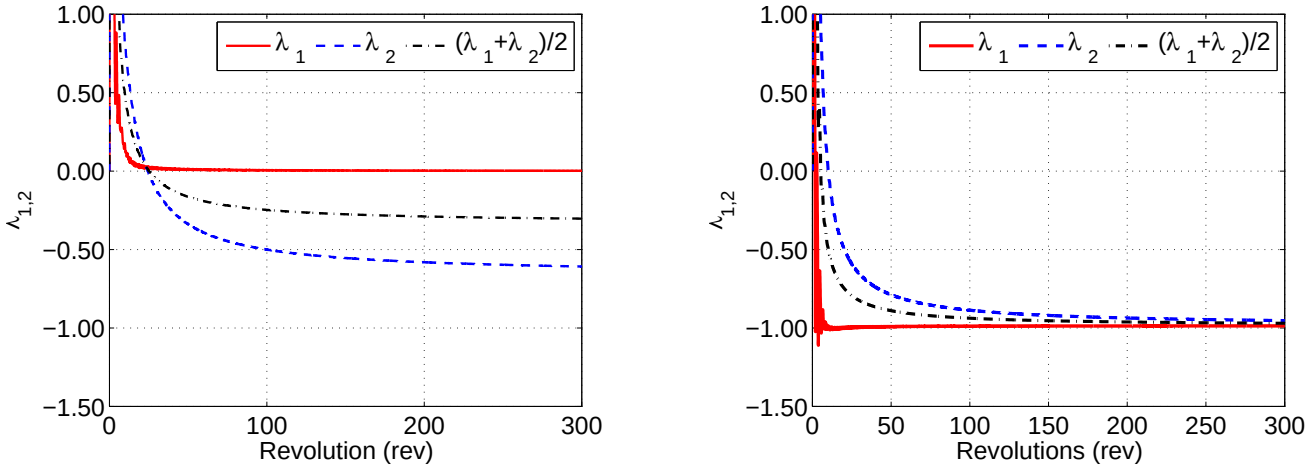

(a) LCO ($C_L = 0$)

(b) Exponentially stable ($C_L = C_d$)

Fig. 6: Helicopter ground resonance with nonlinear blade damper: time evolution of largest two LCE estimates.

Helicopter Ground Resonance with Dissimilar Nonlinear Lead-Lag Dampers

In order to apply the proposed approach to a nonlinear time-dependent problem, one of the dampers of the previous nonlinear damper example is removed from the system to break the symmetry. The linear

term of the damper constitutive law, C_L, is selected as the parameter for the remaining operative dampers. Stability analyses are performed for the range of parameter values considered in the previous example. The two largest LCEs are shown in Fig. 7 as functions of the percentage of linear damping C_L. For C_L/C_d up to 75%, the largest LCE is greater than zero and remaining ones are negative. Since for a nonlinear system a positive LCE indicates chaos, as discussed for example in Ref. 32, a chaotic behavior can be expected in this parameter region. For C_L/C_d greater than 75%, the two largest LCEs merge and both become negative and tend to reduce further, indicating that the fiducial trajectory is now exponentially stable.

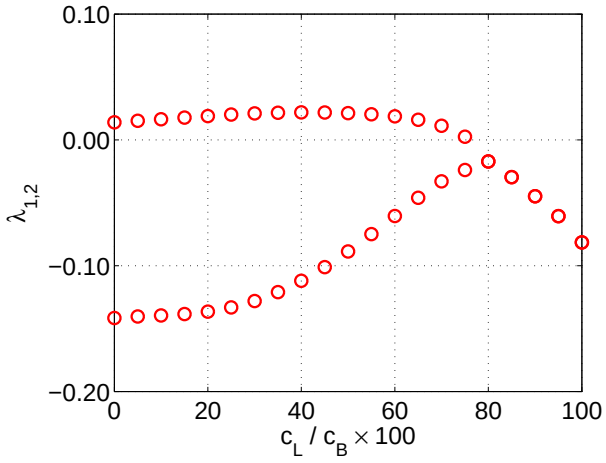

Fig. 7: Helicopter ground resonance with dissimilar nonlinear blade damper: largest two LCE estimates vs. damper slope at zero lag rate C_L.

In order to verify the chaos and stability indications of LCE estimates, we further analyze the two extreme points of Fig. 7. Fig. 8a shows the lag motion of one blade (only one blade is presented for simplicity) for null slope at zero lag rate ($C_L = 0$) compared with the corresponding result of Fig. 4a, i.e. the case of an isotropic rotor with identical nonlinear dampers. The solution appears to be unstable in the sense that it does not converge to an equilibrium point or a periodic orbit but, at the same time, remains within a bounded region of the state space. In fact, this is a distinctive property of chaos, namely a never repeating bounded trajectory, as explained in Refs. 29 and 32. Hence, the presence of a positive largest LCE and the chaotic motion of the blade are in agreement. The time evolution of LCEs for this case, given in Fig. 9a, clearly shows convergence to two separate LCE estimates.

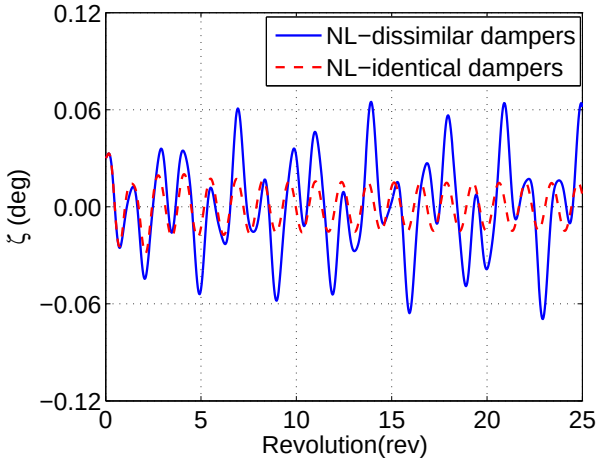

(a) Chaotic ($C_L = 0$)

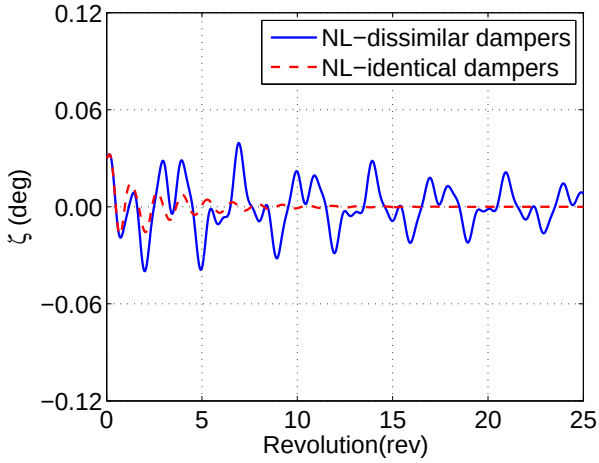

(b) Exponentially stable ($C_L = C_d$)

Fig. 8: Helicopter ground resonance with dissimilar nonlinear blade damper: blade lag motion starting from different initial conditions, compared with the isotropic rotor case.

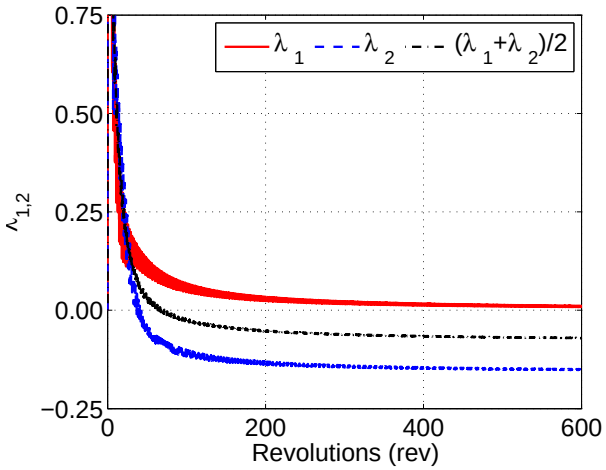

(a) Chaotic ($C_L = 0$)

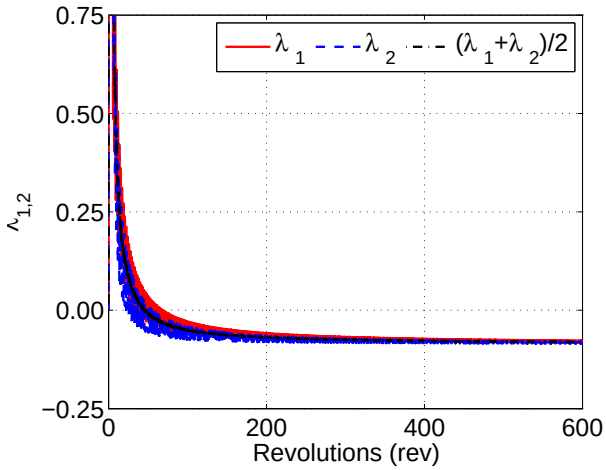

(b) Exponentially stable ($C_L = C_d$)

Fig. 9: Helicopter ground resonance with dissimilar nonlinear blade damper: time evolution of largest two LCE estimates.

On the contrary, Fig. 8b presents the lag motion of one blade for the case of the remaining dampers having nominal slope at zero lag rate ($C_L = C_d$). Again, there appears to be no dominant period in the response, but this time the amplitude (slowly) converges to zero, indicating exponential stability of the

fiducial trajectory. The corresponding evolution in time of the LCE estimates is presented in Fig. 9b, showing two LCEs converging to the same value, thus leading to a largest LCEs with multiplicity 2.

Freeplay Nonlinearity in the Control System

Freeplay is a discontinuity which can occur in control systems; it represents an important source of nonlinearity, which may possibly result in instability, limit cycle oscillations (LCO), and chaotic or quasi-periodic motions in control surfaces. When the position of a control systems falls in the freeplay region, the control is disconnected from its actuation, as it re-connects once the deflection of the control surface exceeds the freeplay limit (Ref. 33). Among the possible mathematical representations, a continuous and differentiable one can be obtained using hyperbolic functions, as done for example in Ref. 34. The proposed function is

$$f_c(\theta) = \frac{1}{2}[1 - \tanh(\varepsilon(\theta - \theta_l))](\theta - \theta_l) + \frac{1}{2}[1 - \tanh(\varepsilon(\theta - \theta_u))](\theta - \theta_u), \tag{20}$$

where θ is the pitch angle, and θ_l and θ_u are the lower and upper boundaries of the freeplay region. The tuning parameter ε determines the accuracy of the representation. A generic example is given in Fig. 10; increased values of ε better represent the nonlinearity.

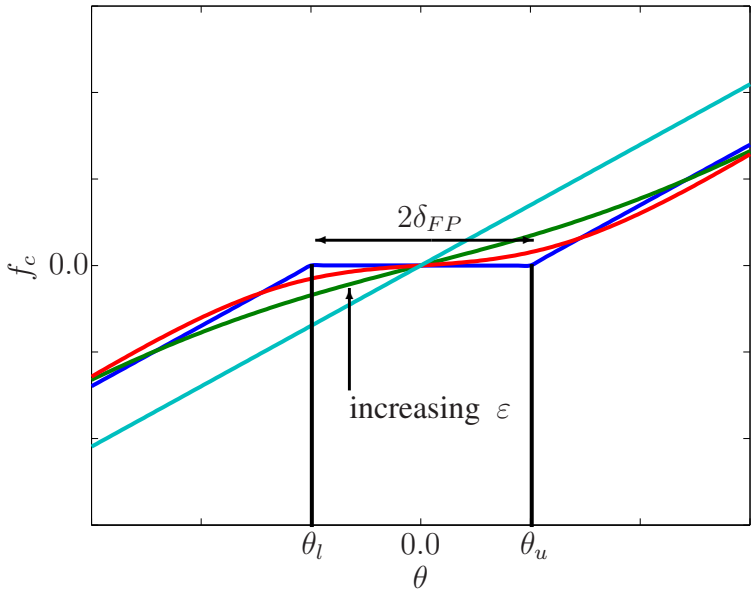

Fig. 10: Freeplay nonlinearity: representation using hyperbolic function.

In Refs. 34 and 35 this hyperbolic representation is used to model the freeplay discontinuity in the classical pitch-plunge aeroelastic model. Chaotic motion and LCO are observed as a consequence of control system freeplay. In rotating blades, even in the absence of control system stiffness, the propeller moment provides residual stiffening effect on the blade pitch rotation. For this reason, pitch-flap coupling is introduced using the δ_3 angle since, as stated in Ref. 36, pitch-flap coupling can result in LCO in tail rotor blades which make use of large values of δ_3 angle to reduce flapping amplitude. This example investigates the detection of limit cycle oscillations using Lyapunov Characteristic Exponents and the verification with the blade response of a tail rotor blade with freeplay nonlinearity and pitch-flap coupling. The tail rotor of the Westland Lynx helicopter is modeled using data from Ref. 37. Unavailable parameters are estimated for a typical tail rotor blade; their values are reported in Table 3.

The coupled aeroelastic pitch-flap equation in non-dimensional form (Ref. 38) is given as:

$$\begin{bmatrix} \hat{I}_\beta & -\hat{I}_x \\ -\hat{I}_x & \hat{I}_f \end{bmatrix} \begin{bmatrix} \ddot{\beta} \\ \ddot{\theta} \end{bmatrix} + \begin{bmatrix} \gamma M_{\dot{\beta}} & \gamma M_{\dot{\theta}} \\ \gamma m_{\dot{\beta}} & \gamma m_{\dot{\theta}} \end{bmatrix} \begin{bmatrix} \dot{\beta} \\ \dot{\theta} \end{bmatrix} + \begin{bmatrix} \hat{I}_\beta \nu_\beta^2 - \gamma M_\beta & -\hat{I}_x - \gamma M_\theta \\ -\hat{I}_x + K_p \hat{I}_f \omega_\theta^2 - \gamma m_\beta & \hat{I}_f(\omega_\theta^2 + 1) - \gamma m_\theta \end{bmatrix} \begin{bmatrix} \beta \\ \theta \end{bmatrix} = 0, \tag{21}$$

where $\hat{I}_\beta$ and $\hat{I}_f$ are the flapping and feathering inertia, non-dimensionalized by $I_b = \int_0^R r^2 m \mathrm{d}r$ for radial coordinate r and mass distribution m; $\hat{I}_x = \int_0^R x_I r m \mathrm{d}r / I_b$ with chordwise center of mass offset x_I; ν_β and ω_θ are non-dimensional flap and pitch frequencies. There is an additional pitch-flap coupling term $K_p = \tan \delta_3$. The aerodynamic terms are weighed with the lock number γ and given in Ref. 38 for the

hover condition as:

$$M_\theta = \frac{1}{8}C'(k_e) \tag{22a}$$

$$M_{\dot\theta} = \frac{c}{24}\left(1 + 2C'(k_e)\left(1 + 2\xi_A\right)\right) \tag{22b}$$

$$M_{\dot\beta} = -\frac{1}{8}C'(k_e)\frac{c^2}{64}\left(1 + 4\xi_A\right) \tag{22c}$$

$$M_\beta = \frac{c}{12}C'(k_e) \tag{22d}$$

$$m_\theta = -\frac{x_A}{6}C'(k_e) \tag{22e}$$

$$m_{\dot\theta} = -\frac{c^2}{32}\left(1 + 4\xi_A\left(1 + 2C'(k_e)\left(1 + 2\xi_A\right)\right)\right) \tag{22f}$$

$$m_{\dot\beta} = \frac{x_A}{6}C'(k_e) - \frac{c^2}{32}\left(\frac{3}{8} + 2\xi_A\left(1 + 2\xi_A\right)\right) \tag{22g}$$

$$m_\beta = -\frac{c^2}{64}\left(1 + 8\xi_A C'(k_e)\right) \tag{22h}$$

where c is the non-dimensional chord, x_A is the non-dimensional aerodynamic center offset, $\xi_A = x_A/c$, and $C'(k_e)$ is the lift deficiency function evaluated at reduced frequency k_e. For simplicity, a quasi-static approximation is assumed in this work, with $C'(k_e) = 1$.

In the model of Eq. (21) the stiffness of the control system is represented by the non-dimensional frequency of the pitching motion about the feathering axis $\hat{I}_f\omega_\theta^2$. In order to introduce freeplay nonlinearity, this term is replaced by the non-dimensional form of the nonlinear constitutive law given in Eq. (20).

In the analysis, a freeplay nonlinearity of 0.10 deg is assumed. The problem is analyzed to compute its LCEs for a range of δ_3 pitch-flap coupling from zero to 45 deg. The stability parameters with ($\delta_{FP} = 0.10$) and without freeplay ($\delta_{FP} = 0.00$) for the prescribed δ_3 range are shown in Fig. 11. The results indicate LCO with zero-valued LCE for the model with freeplay when δ_3 is present. The model without freeplay is exponentially stable for the whole range of the parameter.

The LCO indications using LCEs can be verified by observing the blade response. When the system experiences LCO, the blade motion is expected to approach the same orbit regardless of the initial conditions. Fig. 12 presents the flapping and pitching motions of a blade having 0.10 deg freeplay and with a pitch-flap coupling angle of 30 deg. Although a phase difference can be observed as a consequence of the initial conditions, the blade responses computed from different initial conditions present the same

Table 3: Freeplay: tail rotor characteristics.

Radius*	1.105	m
Chord*	0.18009	m
Lock number*	1.752	—
Pitch-flap coupling*, δ_3	45	deg
Flapping frequency*	1.047	1/rev
Torsional frequency†	2.5	1/rev
Aerodynamic center offset†	0.0	m
Center of mass offset†	0.0	m
Ratio of pitch and flap inertia† $\hat{I}_f/\hat{I}_b$	0.005	—

*Data related to Lynx tail rotor (Ref. 37)

†Assumed parameters

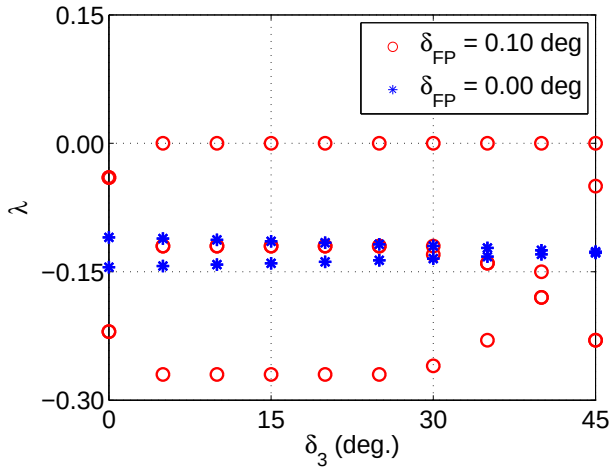

Fig. 11: Freeplay nonlinearity: comparison of LCE estimates with control spring having freeplay ($\delta_{FP} = 0.10$ deg) and without freeplay ($\delta_{FP} = 0.00$ deg).

amplitude and period for both flap and pitch degrees of freedom. This observation confirms the LCO indication given by the presence of a zero-valued largest LCE estimate. The time evolution of the corresponding LCEs can be observed in Fig. 13. Initially, there exist four separate LCE estimates. The largest and the smallest ones converge to separate values, whereas a pair of intermediate LCEs converge to the

same value.

Economy-Size QR Decomposition Example

In order to quantify the potential benefit of using economy-size QR decomposition for LCE estimation, a sample analysis based on the previously mentioned helicopter ground resonance problem with nonlinear

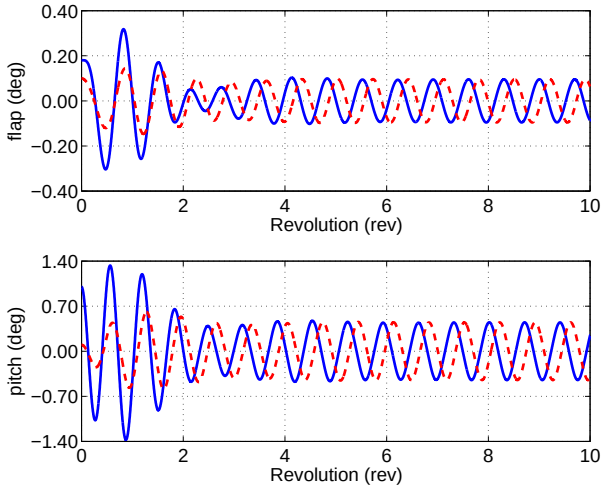

Fig. 12: Freeplay nonlinearity: LCOs of the nonlinear system ($\delta_{FP} = 0.10$ deg) with pitch-flap coupling of $\delta_3 = 30$ deg.

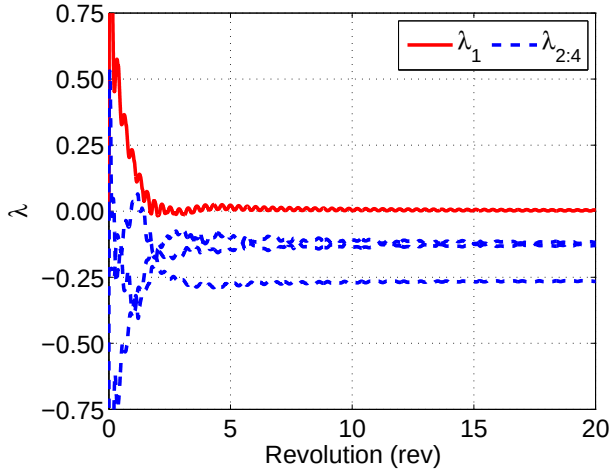

Fig. 13: Freeplay nonlinearity: time Evolution of the LCE estimates of the nonlinear system ($\delta_{FP} = 0.10$ deg) with pitch-flap coupling of $\delta_3 = 30$ deg.

dampers is considered. The size of the problem is n, and q is the number of required LCEs; thus, $q = n$ gives the full QR decomposition case. Fig. 14 shows the time evolution of LCEs for the cases where LCOs exist for $C_L = 0$ (left), and those where the system is exponentially stable $C_L = C_d$ (right). The behavior of the economy QR decomposition for $q = 2$ (represented by $\lambda_{\text{eco},1}$ and $\lambda_{\text{eco},2}$) is very similar to that of the full QR decomposition (λ_1 and λ_2); estimates converge to the same values for both values of C_L.

For the full QR decomposition, the initial conditions matrix $\mathbf{Q}_0$ is the identity, $\mathbf{Q}_0 = \mathbf{I}$, which forms a complete basis. However, when using the economy-size QR decomposition, the initial conditions matrix can only span a subspace of size $q < n$ of the state space, corresponding to the required number of LCE estimates. The selection of the non-zero elements of the initial $\mathbf{Q}'$ matrix, $\mathbf{Q}'_0$, can affect the rate of convergence. A comparison can be made between Figs. 14 and 15, which show two analyses starting from different non-zero elements in matrix $\mathbf{Q}'_0$. While the curves in Fig. 14 present a very good agreement starting from $t = 0$, those in Fig. 15 require more steps to converge. Nevertheless, the LCEs converge to the same results regardless of the initial vectors that are selected in matrix $\mathbf{Q}'_0$.

In order to determine the possible time savings, consider the algorithm for a pre-integrated fiducial trajectory $\mathbf{x}$. The jth step for LCE estimation is

(a) compute the economy-size STM $\mathbf{Y}'_j$ (formally the solution from t_{j-1} to t_j of $\dot{\mathbf{Y}}' = \mathbf{A}(\mathbf{x}(t), t)\mathbf{Y}'$, with $\mathbf{Y}'(t_{j-1}) = \mathbf{Q}'_{j-1}$);

(b) compute the QR decomposition of $\mathbf{Q}'_j\mathbf{R}'_j = \mathbf{Y}'_j$;

(c) update the LCE estimates using $\log(\text{diag}(\mathbf{R}'_{\Pi_j}))$;

(d) go to substep (a).

The main time savings in the algorithm occur in the QR decomposition $\mathbf{Q}'_j\mathbf{R}'_j = \mathbf{Y}_j\mathbf{Q}'_{j-1}$, as the required number of 'flops' (floating point operations) for a QR decomposition is approximately $2nq^2 - 2/3q^3$ (Ref. 23). As a reduced number of LCEs are computed, at each time step $4/3n^3 - 2nq^2 + 2/3q^3$ flops can be saved. Or, put in another way, a fraction $3/2(q/n)^2 - 1/2(q/n)^3$ of the flops required to estimate all LCEs is needed when only q of them are estimated, only counting the flops required for the QR

decomposition. As an example, the time saving in the GR case is shown by calculating the required CPU times corresponding to the number of LCEs estimated using the previously illustrated algorithm, which are reported in Table 4. The reference time (t_r) that is used to normalize the results excludes the QR decomposition, substep (b), but solves the problem for the same time range (substeps (a), (c), and (d)); thus, it corresponds to computing no LCEs, $q = 0$. The results show that non-negligible CPU time can be saved with the implementation of the economy-size QR method. This improvement is important considering the steps required for the estimation of LCEs, especially for large scale problems, when only few of the largest LCEs are required.

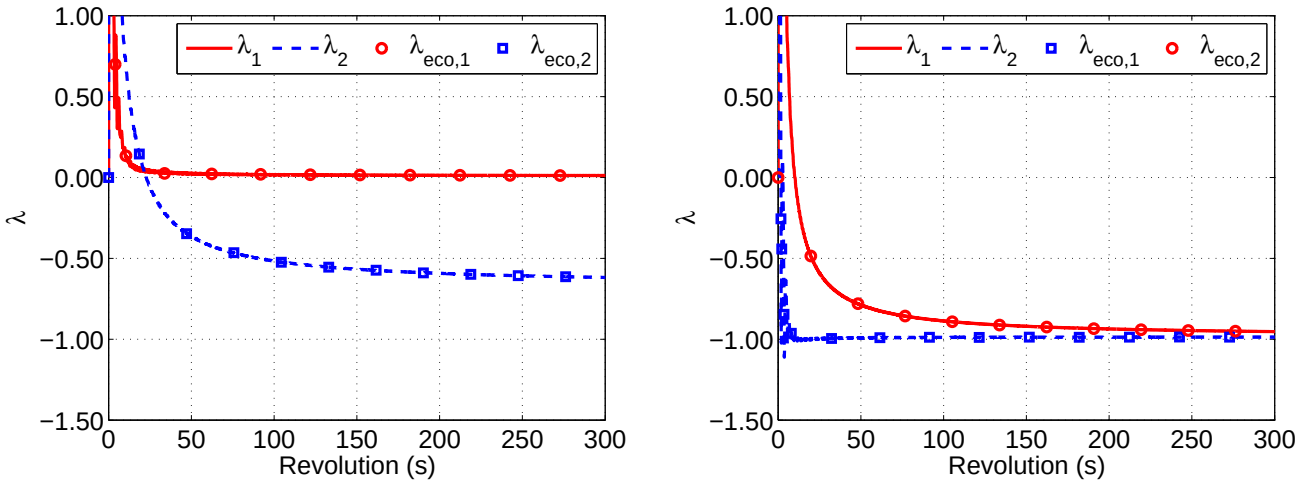

(a) LCO ($C_L = 0$)

(b) Exponentially stable ($C_L = C_d$)

Fig. 14: Comparison of the time evolution of the largest two LCE estimates for complete and economy-size discrete QR method applied to helicopter ground resonance with nonlinear blade damper.

Conclusions

For several aerospace related applications including rotorcraft aeroservoelasticity, time dependence, often in conjunction with non-strict periodicity and quasi-periodicity, as well as nonlinearity, cannot be neglected. A natural generalization of rotorcraft stability analysis using Lyapunov Characteristic Exponents has been presented.

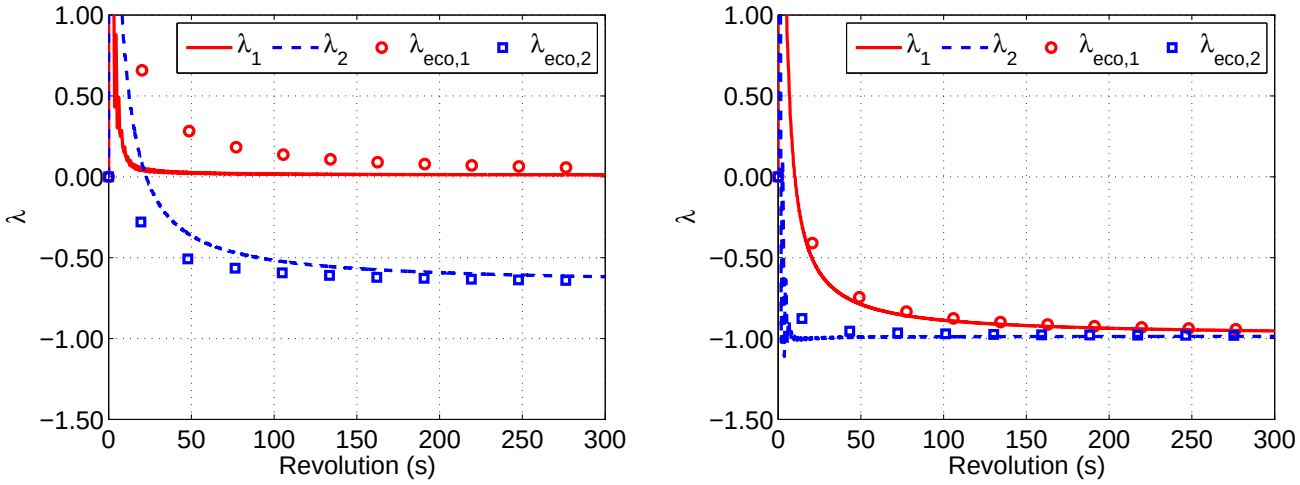

(a) LCO ($C_L = 0$)

(b) Exponentially stable ($C_L = C_d$)

Fig. 15: Comparison of the time evolution of the largest two LCE estimates for complete and economy-size discrete QR method for different values of initial matrix $\mathbf{Q}'_0$.

1) Lyapunov Characteristic Exponents correspond to the real part of the eigenvalues for Linear Time Invariant problems, and to the Floquet exponents for Linear Time Periodic problems; hence, they represent a natural generalization of stability indicators that are familiar in current engineering practice. They extend the definition of spectrum to nonlinear, time-dependent problems.

2) The suitability of the discrete QR algorithm for the practical estimation of Lyapunov Characteristic Exponents has been illustrated.

3) The results of the proposed method have been verified by comparison with corresponding results from linear time invariant and time periodic analyses when possible, and with perturbative analysis of time marching simulations of typical rotorcraft problems of practical interest.

4) Lyapunov Characteristic Exponents estimation may require the computation of long time series resulting from the integration of linear, time variant problems. This process can be substantially longer and more computationally demanding than the one required for conventional stability analysis. Significant time savings can be obtained by using the economy-size QR decomposition to only estimate the largest exponents when large problems are considered.

Table 4: CPU times of economy-size QR decomposition.

q, # of LCEs	Relative computational time
0	1.0000
2	1.0970
4	1.1644
6	1.2183
8	1.3450
10	1.4528
12	1.5876

It is believed that a robust and cost efficient estimation of Lyapunov Characteristic Exponents, with the increasing power of computers, can make this technique a standard stability evaluation practice in the field of rotorcraft aeromechanics.

Appendix: Ground Resonance Equations

Using the classical second-order linear differential equation format, the minimal system of nonlinear equations that governs the ground resonance phenomenon in the non-rotating reference frame can be written as

$$\mathbf{M}\ddot{\mathbf{q}} + \mathbf{C}\dot{\mathbf{q}} + \mathbf{K}\mathbf{q} = \mathbf{m}(\mathbf{q}, \dot{\mathbf{q}}, t), \tag{23}$$

where the vector $\mathbf{q}$ is composed of all the multiblade coordinates and the two components of the helicopters rotor hub displacement x and y. All multiblade coordinates are needed since the problem is nonlinear. In the present case, the nonlinearity is related to the lead-lag dampers. Thus, the complete lead-lag motion is needed to determine the actual amplitude of the lead-lag moment they provide, which is collected in vector $\mathbf{m}$. In the present analysis, a four-blade rotor is considered, without loss of generality. The coordinates vector is thus $\mathbf{q} = \{\zeta_0; \zeta_{1c}; \zeta_{1s}; \zeta_2; x; y\} = \mathbf{T}^{-1}\{\zeta_1; \zeta_2; \zeta_3; \zeta_4; x; y\}$, a transformation from rotating frame to non-rotating frame, where $\mathbf{T}$ being the multi-blade transformation matrix, as explained

in Ref. 39. The matrices are

$$\mathbf{M} = \begin{bmatrix} J_\zeta & 0 & 0 & 0 & 0 & 0 \\ 0 & J_\zeta & 0 & 0 & 0 & S_\zeta \\ 0 & 0 & J_\zeta & 0 & -S_\zeta & 0 \\ 0 & 0 & 0 & J_\zeta & 0 & 0 \\ 0 & 0 & -2S_\zeta & 0 & M_x & 0 \\ 0 & 2S_\zeta & 0 & 0 & 0 & M_y \end{bmatrix} \tag{24}$$

$$\mathbf{C} = \begin{bmatrix} C_L & 0 & 0 & 0 & 0 & 0 \\ 0 & C_L & 2\Omega J_\zeta & 0 & 0 & 0 \\ 0 & -2\Omega J_\zeta & C_L & 0 & 0 & 0 \\ 0 & 0 & 0 & C_L & 0 & 0 \\ 0 & 0 & 0 & 0 & C_x & 0 \\ 0 & 0 & 0 & 0 & 0 & C_y \end{bmatrix} \tag{25}$$

$$\mathbf{K} = \begin{bmatrix} K_d & 0 & 0 & 0 & 0 & 0 \\ 0 & K_d - \Omega^2 J_\zeta & \Omega C_L & 0 & 0 & 0 \\ 0 & -\Omega C_L & K_d - \Omega^2 J_\zeta & 0 & 0 & 0 \\ 0 & 0 & 0 & K_d & 0 & 0 \\ 0 & 0 & 0 & 0 & K_x & 0 \\ 0 & 0 & 0 & 0 & 0 & K_y \end{bmatrix} \tag{26}$$

$$\mathbf{m} = -\mathbf{T}^{-1} \begin{Bmatrix} f_{dq,1} \\ f_{dq,4} \\ f_{dq,4} \\ f_{dq,4} \\ 0 \\ 0 \end{Bmatrix} = - \begin{Bmatrix} \frac{1}{4}(f_{dq,1} + f_{dq,2} + f_{dq,3} + f_{dq,4}) \\ -\frac{\sin\psi}{2} f_{dq,1} - \frac{\cos\psi}{2} f_{dq,2} + \frac{\sin\psi}{2} f_{dq,3} + \frac{\cos\psi}{2} f_{dq,4} \\ \frac{\cos\psi}{2} f_{dq,1} - \frac{\sin\psi}{2} f_{dq,2} - \frac{\cos\psi}{2} f_{dq,3} + \frac{\sin\psi}{2} f_{dq,4} \\ \frac{1}{4}(-f_{dq,1} + f_{dq,2} - f_{dq,3} + f_{dq,4}) \\ 0 \\ 0 \end{Bmatrix}. \tag{27}$$

where, in addition to all the parameters defined in Tables 1 and 2, ψ is the azimuth angle of the first blade, and $f_{dq,i}$ is the quadratic part of the nonlinear damping moment given in Eq. (19) that corresponds to the ith blade.

References

[1]Lyapunov, A. M., *The General Problem of the Stability of Motion*, Taylor & Francis, Translated and edited by A. T. Fuller, 1992.

[2]Perko, L., *Differential Equations and Dynamical Systems*, Texts in Applied Mathematics, Springer, New York, third edition, 2001.

[3]Roberts, A. J., "The application of centre-manifold theory to the evolution of system which vary slowly in space," *The Journal of the Australian Mathematical Society. Series B. Applied Mathematics*, Vol. 29, (04), doi:10.1017/S0334270000005968, April 1988, pp. 480–500.

[4]Parkus, H., "The Disturbed Flapping Motion of Helicopter Rotor Blades," *Journal of the Aeronautical Sciences*, Vol. 15, (2), doi:10.2514/8.11513, 1948, pp. 103–106.

[5]Peters, D. A. and Hohenemser, K. H., "Application of the Floquet Transition Matrix to Problems of Lifting Rotor Stability," *Journal of the American Helicopter Society*, Vol. 16, (2), doi:10.4050/JAHS.16.25, 1971, pp. 25–33.

[6]Hammond, C. E., "An Application of Floquet Theory to Prediction of Mechanical Instability," *Journal of the American Helicopter Society*, Vol. 19, (4), doi:10.4050/JAHS.19.14, 1974, pp. 14–23.

[7]Biggers, J. C., "Some Approximations to the Flapping Stability of Helicopter Rotors," *Journal of the American Helicopter Society*, Vol. 19, (4), doi:10.4050/JAHS.19.24, 1974, pp. 24–33.

[8]Friedmann, P. and Silverthorn, J., "Aeroelastic Stability of Periodic Systems with Application to Rotor Blade Flutter," AIAA/ASME/SAE 15th Structures, Structural Dynamics and Materials Conference, April 17–19 1974.

[9]Bielawa, R. L., *Rotary Wing Structural Dynamics and Aeroelasticity*, AIAA, Washington, DC, second edition, 2005.

[10]Jones, M., Bernascone, A., Masarati, P., Quaranta, G., and Rezgui, D., "Ongoing Developments in

the Use of Continuation-Bifurcation Methodology at AgustaWestland," 40th European Rotorcraft Forum, September 2–5 2014.

[11]Tamer, A. and Masarati, P., "Do We Really Need To Study Rotorcraft as Linear Periodic Systems?" AHS 71th Annual Forum, May 5–7 2015.

[12]Benettin, G., Galgani, L., Giorgilli, A., and Strelcyn, J.-M., "Lyapunov characteristic exponents for smooth dynamical systems and for Hamiltonian systems; a method for computing all of them. Part 1: Theory," *Meccanica*, Vol. 15, (1), doi:10.1007/BF02128236, March 1980, pp. 9–20.

[13]Geist, K., Parlitz, U., and Lauterborn, W., "Comparison of Different Methods for Computing Lyapunov Exponents," *Progress of Theoretical Physics*, Vol. 83, (5), doi:10.1143/PTP.83.875, May 1990, pp. 875–893.

[14]Dieci, L. and Van Vleck, E. S., "Lyapunov Spectral Intervals: Theory and Computation," *SIAM Journal on Numerical Analysis*, Vol. 40, (2), doi:10.1137/S0036142901392304, 2002, pp. 516–542.

[15]Dieci, L., Jolly, M. S., and Van Vleck, E. S., "Numerical Techniques for Approximating Lyapunov Exponents and Their Implementation," *J. of Computational and Nonlinear Dynamics*, Vol. 6, (1), doi:10.1115/1.4002088, 2010, pp. 011003.

[16]Cong, N. D. and Nam, H., "Lyapunov's Inequality for Linear Differential Algebraic Equation," *Acta Mathematica Vietnamica*, Vol. 28, (1), 2003, pp. 73–88.

[17]Cong, N. D. and Nam, H., "Lyapunov Regularity of Linear Differential Algebraic Equations of Index 1," *Acta Mathematica Vietnamica*, Vol. 29, (1), 2004, pp. 1–21.

[18]Linh, V. H. and Mehrmann, V., "Lyapunov, Bohl and Sacker-Sell Spectral Intervals for Differential-Algebraic Equations," *J. Dyn. Diff. Equat.*, Vol. 21, doi:10.1007/s10884-009-9128-7, 2009, pp. 153–194.

[19]Linh, V. H. and Mehrmann, V., "Approximation of Spectral Intervals and Leading Directions for Differential-Algebraic Equation via Smooth Singular Value Decompositions," *SIAM Journal on Numerical Analysis*, Vol. 49, (5), doi:10.1137/100806059, 2011, pp. 1810–1835.

[20]Linh, V., Mehrmann, V., and Van Vleck, E., "QR methods and error analysis for computing Lyapunov and Sacker-Sell spectral intervals for linear differential-algebraic equations," *Advances in Computational Mathematics*, Vol. 35, (2–4), doi:10.1007/s10444-010-9156-1, 2011, pp. 281–322.

[21]Masarati, P., "Estimation of Lyapunov Exponents from Multibody Dynamics in Differential-Algebraic Form," *Proc. IMechE Part K: J. Multi-body Dynamics*, Vol. 227, (4), doi:10.1177/1464419312455754, 2013, pp. 23–33.

[22]Golub, G. H. and Van Loan, C. F., *Matrix Computations*, The Johns Hopkins University Press, Baltimore and London, third edition, 1996.

[23]Trefethen, L. N. and Bau, D., *Numerical Linear Algebra*, SIAM, Philadelphia, 1997.

[24]Van Vleck, E. S., Dieci, L., and Jolly, M., "Codes for Approximating Lyapunov Exponents," ASME IDETC/CIE 2009, DETC2009–86530, August 30–September 2 2009.

[25]Masarati, P., Morandini, M., and Mantegazza, P., "An efficient formulation for general-purpose multibody/multiphysics analysis," *J. of Computational and Nonlinear Dynamics*, Vol. 9, (4), doi:10.1115/1.4025628, 2014, pp. 041001.

[26]Peters, D. A., Lieb, S. M., and Ahaus, L. A., "Interpretation of Floquet Eigenvalues and Eigenvectors for Periodic Systems," *Journal of the American Helicopter Society*, Vol. 56, (3), doi:10.4050/JAHS.56.032001, July 2011, pp. 1–11.

[27]Coleman, R. P. and Feingold, A. M., "Theory of Self-Excited Mechanical Oscillations of Helicopter Rotors with Hinged Blades," Report 1351, NACA, 1958.

[28]Tamer, A. and Masarati, P., "Helicopter Rotor Aeroelastic Stability Evaluation Using Lyapunov Exponents," 40th European Rotorcraft Forum, September 2–5 2014.

[29]Strogatz, S. H., *Nonlinear Dynamics and Chaos: With Applications to Physics, Biology, Chemistry, and Engineering*, Perseus Books, Reading, Massachusetts, 1994.

[30]Hodges, D. and Pierce, G. A., *Introduction to Structural Dynamics and Aeroelasticity*, Cambridge University Press, Cambridge, England, 2002.

[31]Quaranta, G., Muscarello, V., and Masarati, P., "Lead-Lag Damper Robustness Analysis for Helicopter Ground Resonance," *J. of Guidance, Control, and Dynamics*, Vol. 36, (4), doi:10.2514/1.57188, July 2013, pp. 1150–1161.

[32]Medio, A. and Lines, M., *Nonlinear Dynamics — A Primer*, Cambridge University Press, 2001.

[33]Eller, D., "Friction, Freeplay and Flutter of Manually Controlled Aircraft," International Forum on Aeroelasticity and Structural Dynamics, June 2007.

[34]Vasconcellos, R., Abdelkefi, A., Marques, F., and Hajj, M., "Representation and analysis of control surface freeplay nonlinearity," *Journal of Fluids and Structures*, Vol. 31, doi:10.1016/j.jfluidstructs.2012.02.003, 2012, pp. 79–91.

[35]Vasconcellos, R., Abdelkefi, A., Hajj, M. R., and Marques, F., "Discontinuity induced bifurcation in aeroelastic systems with freeplay nonlinearity," 22nd International Congress of Mechanical Engineering (COBEM'13), November 3–7 2013.

[36]Bramwell, A. R. S., Done, G., and Balmford, D., *Bramwell's Helicopter Dynamics*, Butterworth-Heinemann, 2001.

[37]Lau, B. H., Louie, A. W., Griffiths, N., and Sotiriou, C. P., "Performance and Rotor Loads Measurements of the Lynx XZ170 Helicopter with Rectengular Blades," TM 104000, NASA, 1993.

[38]Johnson, W., *Rotorcraft Aeromechanics*, Cambridge University Press, 2013.

[39]Bir, G., "Multiblade Coordinate Transformation and Its Application to Wind Turbine Analysis," ASME Wind Energy Symposium, NREL/CP-500-42553, January 7–10 2008.